# Computational Chemistry of Modified $[MFe_3S_4]$ and $[M_2Fe_2S_4]$ Clusters: Assessment of Trends in Electronic Structure and Properties†

**Kasper P. Jensen,* Bee-Lean Ooi, and Hans E. M. Christensen**

*Department of Chemistry, Technical University of Denmark, Building 207, 2800 Kgs. Lyngby, DK - Denmark*

*Received: February 19, 2008; Revised Manuscript Received: May 26, 2008*

The aim of this work is to understand the molecular evolution of iron−sulfur clusters in terms of electronic structure and function. Metal-substituted models of biological $[Fe_4S_4]$ clusters in oxidation states $[M_xFe_{4-x}S_4]^{3+/2+/1+}$ have been studied by density functional theory (M = Cr, Mn, Fe, Co, Ni, Cu, Zn, and Pd, with $x = 1$ or 2). Most of these clusters have not been characterized before. For those that have been characterized experimentally, very good agreement is obtained, implying that also the predicted structures and properties of new clusters are accurate. Mean absolute errors are 0.024 Å for bond lengths ($[Fe_4S_4]$, $[NiFe_3S_4]$, $[CoFe_3S_4]$) and 0.09 V for shifts in reduction potentials relative to the $[Fe_4S_4]$ cluster. All structures form cuboidal geometries similar to the all-iron clusters, except the Pd-substituted clusters, which instead form highly distorted trigonal and tetragonal local sites in compromised, pseudocuboidal geometries. In contrast to other electron-transfer sites, cytochromes, blue copper proteins, and smaller iron−sulfur clusters, we find that the $[Fe_4S_4]$ clusters are very insensitive to metal substitution, displaying quite small changes in reorganization energies and reduction potentials upon substitution. Thus, the $[Fe_4S_4]$ clusters have an evolutionary advantage in being robust to pollution from other metals, still retaining function. We analyze in detail the electronic structure of individual clusters and rationalize spin couplings and redox activity. Often, several configurations are very close in energy, implying possible use as spin-crossover systems, and spin states are predicted accurately in all but one case ($[CuFe_3S_4]$). The results are anticipated to be helpful in defining new molecular systems with catalytic and magnetic properties.

## Introduction

This paper reports computational investigations of hetero-metal-substituted iron−sulfur clusters $[MFe_3S_4]$ and $[M_2Fe_2S_4]$ and describes their properties in detail, including geometries, reduction potentials, inner-sphere reorganization energies, atomic spins and charges, and trends in redox- and heterometal-dependent electronic structures and spin-coupling modes. A particular focus is directed toward understanding whether modifications of the $[Fe_4S_4]$ framework are structurally stable and functional, as compared to nature's preferred choice.

The use of iron−sulfur clusters in proteins can hardly be overappreciated; with their simple forms, some depicted in Figure 1, their diverse functions include electron transfer, ligand binding and activation, structural roles, sensing, and regulation.[1,2] This immense diversity in function, the relatively small size and easy access, and the apparent early use in biology[3] render these proteins ideal as templates for design of artificial bioinspired catalysts. This can be achieved by using building blocks of both bioavailable and unavailable metals and ligands, thereby going beyond the constraints enforced through biomolecular evolution. It is our ongoing project to understand in detail the fundamental electronic structure and the potential new functions of modified iron−sulfur clusters, elucidating how these simple systems can be so multifunctional and also to help us outline the design principles of new, bioinspired minimal-model catalysts.

Heterometal-substituted iron−sulfur clusters in proteins have been made from $[Fe_3S_4]$ clusters, which can be derived from

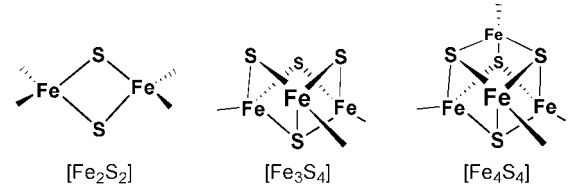


**Figure 1.** Some iron−sulfur clusters found in nature.

$[Fe_4S_4]$ clusters in a variety of proteins.[4,5] These new heterometallic clusters are assumed or, in a few cases, known to form stable cuboidal structures similar to the native all-iron forms and display altered magnetic and electrochemical properties.[4] The general understanding of the rather complex electronic structure of iron−sulfur clusters was greatly helped by introducing the concept of antiferromagnetic spin−spin coupling and valence delocalization when rationalizing magnetic data.[4,6] These concepts remain important tools for understanding and designing new modified iron−sulfur-like clusters with altered functionality, and for this reason, computation can ideally lead the way for experimental long-term efforts in this area.

Computational chemistry of transition-metal systems has been revolutionized by the advent of density functional theory (DFT),[7–9] which is now considered the golden standard for obtaining geometries and energies of similar electronic configurations in transition-metal systems, with errors of ∼0.02 Å for diatomic metal−ligand bonds,[10] 30 kJ/mol (∼0.4 eV) for ionization energies, and 40 kJ/mol for bond dissociation energies,[10] or down to 20 kJ/mol for other types of reaction energies.[11,12] Furthermore, earlier work indicates that inner-sphere reorganization energies can be accurate to ∼10 kJ/mol[13] due to cancelation of errors when subtracting energies of the

† Part of the "Sason S. Shaik Festschrift".

* To whom correspondence should be addressed. E-mail: kpj@kemi.dtu.dk.

10.1021/jp8014782 CCC: $40.75 
Published on Web 07/09/2008

same electronic configuration at different points of the potential energy surface.

At the same time, there is much evidence that the relative energies of configurations involving substantial changes in orbital occupation, and thus representing distinctly different electron correlation effects,[14,15] are inherently difficult to treat consistently with DFT, as different functionals will bias different configurations. A particular challenging problem involves energies of configurations with a different excess number of unpaired electrons ($M_S$ quantum number)[14] and bond dissociation energies (BDE),[16] with hybrid functionals such as B3LYP well-known to favor the open-shell, spin-polarized cases as compared to generalized gradient approximation (GGA) functionals such as BP86.[16]

In iron−sulfur clusters, as will be clear, spin states lie very close in energy, adding to the complexity but also increasing their potential use as, for example, molecular magnets and ligand-binding systems. In this context, it has been shown that close-lying spin states serve an important role in allowing oxygen-based ligands to bind to heme systems.[17–19] These results indicated that spin state energies together with metal−ligand BDEs serve as important descriptors for rational design of catalysts, that is, catalytic activity can be obtained by designing biomimetic systems with close-lying spin states which can, at the same time, bind small ligands, activate them, and subsequently catalyze the degradation of substrates.

Earlier work in this direction includes recent computational studies of modified [Fe], [$Fe_2S_2$],[13] and [$Fe_3S_4$] clusters,[20] which could account for nature's choice of all-iron centers as the preferred motif for electron transfer. Other recent work showed that simple modifications of amino acid ligands can lead to substantial effects in the structure and function of proteins, as witnessed in *P. furiosus* ferredoxin,[21] where the coordinating aspartate serves as a trigger: This residue can selectively stabilize reduced and oxidized states by shifting between a weakly donating monodentate and a strongly donating bidentate coordination mode,[21] a property which cysteine does not possess.

We will show here that similar fundamental insight can be obtained from computational studies of modified [$Fe_4S_4$] clusters. This is of importance not only due to the widespread occurrence of this cluster type in biology and for understanding their properties by defining the chemical alternatives but also because the [$Fe_4S_4$] clusters are ideal experimental templates for future attempts at designing simple molecular systems with new properties.

## Methods

**Model Systems.** All models applied in this work consisted of the cuboidal core with four metal ions, four inorganic sulfides, and four thiolate groups as models of cysteinates, as shown in Figure 2. Atoms have been numbered according to their designations in the text. The clusters represent minimal models that, in an ideal way, account for intrinsic properties of the cofactors, whereas environmental effects can vary and change properties substantially and in a nonsystematic manner. The clusters are referred to by stating the four metals, the four sulfide atoms, and the charge of this core, that is, $[Fe_4S_4]^+$ in the most reduced form and $[Fe_4S_4]^{3+}$ in the most oxidized state. Alternatively, the total charge $Q$ (including cysteinates) of each cluster is used, which ranges from $Q = -3$ to $-1$, corresponding to between one and three trivalent metal ions, the rest formally being divalent. Geometries were optimized based on the computed structure of the native [$Fe_4S_4$] cluster, which was shown to be in good structural agreement with experiment (see Results and Discussion).

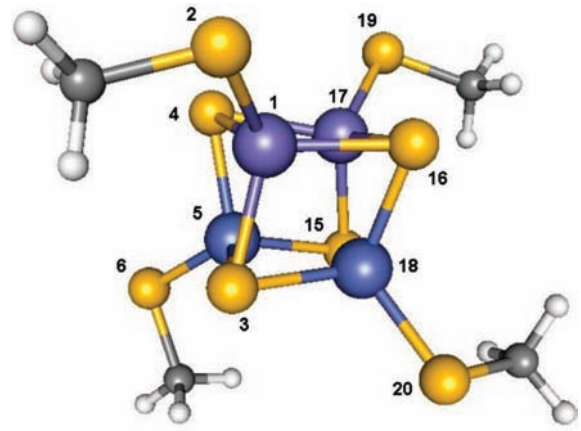


**Figure 2.** Stoichiometry and nomenclature of computational models investigated in this work. Hydrogens are shown in white, carbons in black, sulfurs in yellow, and metals in blue.

**Computational Details.** DFT should, in principle, be capable of describing accurately all observables related to iron−sulfur clusters and thus be of invaluable use in the search for new catalysts by computing optimal properties, but this assumes a physically correct functional, which is not trivially available. Many properties, in addition to geometries, can be computed with high accuracy using DFT, including redox potentials for [Fe], [$Fe_2S_2$], and [$Fe_4S_4$] clusters[22–25] and for full proteins,[26] reorganization energies,[27,28] transmission coefficients,[29] and NMR parameters.[30] However, no universally perfect functional exists, and problems related to relative energies and thus insight into reactivity persist. The so-called broken-symmetry (BS) approach[31–34] has been used to obtain values of spin-coupling constants for spin-coupled transition-metal systems. The approach uses the difference between the maximum spin and BS low-spin configurations as an estimate of the spin-coupling constant $J$ in a Heisenberg Hamiltonian. The BS singlet is not a true singlet and thus not an eigenfunction to the Heisenberg Hamiltonian (the maximum spin KS determinant is approximately so), and $J$ constants remain hugely sensitive to functional, as they scale linearly with the spin-splitting energy, and thus do not solve any problem quantitatively. However, computing the energy difference between the maximum spin and the BS low-spin configuration is generally a good way to access the sign of $J$ (ferromagnetic versus antiferromagnetic coupling). Our preferred approach is to compute energies of configurations with varying $M_S$ quantum number and compare these to assess the nature of the ferromagnetic coupling.

It has been seen that, although relative energies of different $M_S$ configurations vary, several GGA and hybrid functionals still reproduce the qualitatively correct spin state of small transition-metal systems, with no clearly superior functional available.[10] However, on the basis of earlier experience and assessment of accuracy,[10,16,20,21] the Becke 1988 exchange functional combined with the Perdew 1986 nonlocal correlation functional (BP86)[35,36] was used.

The calculations were carried out with the Turbomole program,[37] version 5.8. Only the pure five d- and seven f-type functions were used. All optimizations were carried out in redundant internal coordinates using the Cosmo model (vide infra). Fully unrestricted calculations were performed for all Kohn−Sham (KS) configurations. We made use of the default convergence criteria, which imply self-consistency down to $10^{-6}$

Hartree (2.6 J/mol) for the electronic energy and $10^{-3}$ au for the largest acceptable norm of the gradient. The basis sets used for geometry optimization were 6-31G(d) for all atoms, whereas metal ions were assigned a TZVP basis set.[38] This basis set size was chosen because our past experience indicates that it represents a reasonable compromise between speed and accuracy when studying large combinatorial sets of molecules, as is the case in this work.

To further access the accuracy of the procedure, we evaluated the effect upon increasing the size of the basis set to 6-311+G(2d,2p), which includes diffuse functions and a better account of radial electron correlation in the clusters. Although this approach is not computationally feasible for all clusters due to the size of the basis sets, we have computed the self-exchange reorganization energies for a test set of the [$Fe_4S_4$], [$MnFe_3S_4$], [$CoFe_3S_4$], and [$NiFe_3S_4$] clusters and also computed energies with two other functionals, B3LYP and TPSSh, incorporating 20 and 10% exact exchange, respectively. The results in Supporting Information Tables S1−S4 show that maximum deviations of 12 kJ/mol and MADs of 5 kJ/mol are obtained when using the two basis sets with the BP86 functional. Similar differences are observed when using other functionals. These relatively small differences justify our approach, given that the self-exchange reorganization energies are crucial to the conclusions of this work. The small deviations are due to the fact that the self-exchange reorganization energies are composed of four electronic energies, two of which represent oxidized states and two reduced states; this gives rise to a large degree of error cancelation since the radial correlation effects in the two types of states cancel each other.

The spin quantum number $S$ is not well-defined for unrestricted KS determinant wave functions due to spin contamination,[39–41] but the difference in the number of α- and $\beta$-electrons occupied in the KS determinant defines the $M_S$ value. Often, the highest possible $M_S$ values are lowest in energy because of the exchange correlation energy, in accordance with Hund's Rule. The highest $M_S$ value coincides with the $S$ quantum number, so when this configuration is found to have the lowest energy, there is only one $S$ value corresponding to it, namely, $S = M_S$. In such cases, the molecule can be expected to have a high-spin ground state, and the KS determinant is a good approximation to this state. However, other real states are comprised of more configurations, of which only the one determinant giving the lowest local energy minimum is pursued in the DFT formalism.

In the case of iron−sulfur clusters, there is always a substantial antiferromagnetic spin coupling causing the ground state to have a fairly small $M_S$ quantum number: These systems consist of oppositely aligned sites of local high-spin configurations (i.e., open-shell low-spin configurations from unrestricted DFT (UDFT) or Hartree−Fock (UHF), sometimes referred to as BS configurations). Characteristic of them are small $M_S$ values but large estimates of $<S^2>$, indicating correctly that higher-spin components are present in the KS determinant. To localize and optimize these electronic structures, it is usually necessary to begin from a high-spin configuration, which is easier to converge, and then gradually flip the spins of the electrons in the configurations, using the previously optimized orbitals as starting orbitals for the optimization of spin-down coupled states. This tedious procedure can be performed systematically and ultimately leads to well-converged antiferromagnetic KS configurations, which are then geometry optimized individually to obtain a true minimum on the potential energy surface for each electronic configuration. We have reported energies for the fully antiferromagnetic configurations with $M_S = M_{S0} = 1/2$ for systems with an odd number of d electrons or 0 for systems with an even number of d electrons, as well as for configurations with $M_S = M_{S0} + 1$ and 2.

**Cosmo Energies.** Due to the importance of electrostatic shielding in any highly charged cluster, the Conductor-Like Screening Model (Cosmo)[42,43] was used for computation of all energies. In this method, the solute molecule forms a cavity within a dielectric continuum characterized by a dielectric constant, $\varepsilon$. The charge distribution of the solute polarizes the dielectric medium, and the response of the medium is described by the generation of screening charges on the surface of the cavity. These calculations were performed with a dielectric constant of 80, similar to water, as these systems will most often be studied experimentally in polar solvents. The value found in proteins is estimated at 4−16.[44] Environmental effects can affect energetics substantially, but in the present work, we are concerned with intrinsic properties of the isolated clusters and thus study them in a more polar model.

For the generation of the cavity, a set of atomic radii has to be defined. The optimized Cosmo radii in Turbomole were applied (H: 1.30 Å, C: 2.00 Å, S: 2.16 Å).[45] The radii for all metals were set to 2.0 Å. We know from earlier studies[20,21] that absolute Cosmo energies vary by less than 6 kJ/mol when changing the metal radius due to the essentially buried metal ion and that relative effects are even smaller, that is, only up to a few kJ/mol.

Reduction potentials were derived from eq 1

$$E^0 = E^{\mathrm{Cosmo}}(\mathrm{ox}) - E^{\mathrm{Cosmo}}(\mathrm{red}) - 4.43\ \mathrm{eV} \qquad (1)$$

where the factor of 4.43 eV represents the potential of the standard hydrogen electrode.[46] Only relative potentials of clusters are considered reliable since different proteins and environmental effects can change the absolute potentials substantially but usually in a uniform way. The shifts in reduction potential accompanying the change of metal in the clusters turns out to be accurately described by this procedure to within ∼0.09 V (see Results and Discussion), corresponding to a standard error of ∼10 kJ/mol, which is accurate enough to draw significant conclusions and justifies the computational chemistry setup of this work.

## Results and Discussion

**Spin States.** As described above,[11,47] whereas the spin of the ground state can usually be predicted with some success, the energy gap between states is critically dependent on the type of functional used. Table 1 contains the relative energies of antiferromagnetically coupled configurations with maximal spin pairing (lowest $M_S$ quantum number, $M_{S0}$) and the next two configurations of partial spin pairing ($M_{S0+1}$ and $M_{S0+2}$), which can arise in the heterometallic clusters when a metal is localized and has weak coupling with the other metal sites. The configuration with the lowest electronic energy implies which $M_S$ quantum number is likely to describe the ground state of the cluster. We have compared our results with the spin states deduced for heterometallic clusters in *P. furiosus* ferredoxin. Although one of the four ligands is Asp in this protein, it can be assumed that the electronic configurations are very similar, as indicated from computations of all-iron clusters with Ser, Cys, and Asp ligands,[21] and thus, the protein data serve as a reference point for confirming how reasonable the computations are in each case. Whereas this section deals with identifying the ground states of the clusters, the details of the electronic structures will be discussed later in a separate section.

**TABLE 1: Energies of Electronic Configurations and Computed and Experimental Spins**

| cluster | | | | | $E_{el}$ (kJ/mol)[a] | | | spin | |
|---|---|---|---|---|---|---|---|---|---|
| M1 | M5 | M17 | M18 | $Q$ | $M_{S0}$ | $M_{S0}+1$ | $M_{S0}+2$ | computed | experiment[4,b] |
| Fe | Fe | Fe | Cr | −3 | 0 | 6 | 41 | 1/2, 3/2 | 3/2[48] |
| Fe | Fe | Fe | Cr | −2 | 37 | 0 | 12 | 1 | EPR silent[48] |
| Fe | Fe | Fe | Cr | −1 | 0 | 5 | 47 | 1/2, 3/2 | |
| Fe | Fe | Cr | Cr | −3 | 0 | 33 | 57 | 1/2 | |
| Fe | Fe | Cr | Cr | −2 | 0 | 9 | 23 | 0, 1 | |
| Fe | Fe | Cr | Cr | −1 | 0 | 6 | 38 | 1/2, 3/2 | |
| Fe | Fe | Fe | Mn | −3 | 0 | 32 | 86 | 0 | 0[49] |
| Fe | Fe | Fe | Mn | −2 | 0 | 59 | 39 | 1/2 | |
| Fe | Fe | Fe | Mn | −1 | 1 | 0 | 1 | 0, 1, 2 | |
| Fe | Mn | Fe | Mn | −3 | 0 | 55 | 110 | 1/2 | |
| Fe | Mn | Fe | Mn | −2 | 0 | 53 | 36 | 0 | |
| Fe | Mn | Fe | Mn | −1 | 0 | 8 | 14 | 1/2, 3/2 | |
| Fe | Fe | Fe | Fe | −3 | 0 | 39 | 53 | 1/2 | 1/2, 3/2[50] |
| Fe | Fe | Fe | Fe | −2 | 0 | 49 | 70 | 0 | 0[50] |
| Fe | Fe | Fe | Fe | −1 | 0 | 31 | 31 | 1/2 | |
| Fe | Fe | Fe | Co | −3 | 18 | 0 | 95 | 1 | 1[49] |
| Fe | Fe | Fe | Co | −2 | 0 | 72 | 56 | 1/2 | 1/2[49] |
| Fe | Fe | Fe | Co | −1 | 0 | 18 | 44 | 0 | |
| Fe | Co | Fe | Co | −3 | 30 | 0 | 39 | 3/2 | |
| Fe | Co | Fe | Co | −2 | 57 | 22 | 0 | 2 | |
| Fe | Co | Fe | Co | −1 | 0 | 26 | 31 | 1/2 | |
| Fe | Fe | Fe | Ni | −3 | 26 | 0 | 15 | 3/2 | 3/2[51] |
| Fe | Fe | Fe | Ni | −2 | 13 | 0 | 19 | 1 | |
| Fe | Fe | Fe | Ni | −1 | 0 | 9 | 26 | 1/2, 3/2 | |
| Fe | Fe | Ni | Ni | −3 | 0 | 36 | 4 | 1/2, 5/2 | |
| Fe | Fe | Ni | Ni | −2 | 0 | 22 | 0 | 0, 2 | |
| Fe | Fe | Ni | Ni | −1 | 0 | 9 | 13 | 1/2, 3/2 | |
| Fe | Fe | Fe | Cu | −3 | 73 | 34 | 0 | 2 | 2[48] |
| Fe | Fe | Fe | Cu | −2 | 14 | 0 | 20 | 3/2 | 1/2[48] |
| Fe | Fe | Fe | Cu | −1 | 8 | 0 | 23 | 0, 1 | |
| Fe | Fe | Cu | Cu | −3 | 0 | 38 | 26 | 1/2 | |
| Fe | Fe | Cu | Cu | −2 | 7 | 9 | 0 | 0, 1, 2 | |
| Fe | Fe | Cu | Cu | −1 | 12 | 8 | 0 | 3/2, 5/2 | |
| Fe | Fe | Fe | Zn | −3 | 53 | 11 | 0 | 5/2 | 5/2[49,52] |
| Fe | Fe | Fe | Zn | −2 | 49 | 26 | 0 | 2 | 2[49,52] |
| Fe | Fe | Fe | Zn | −1 | 13 | 0 | 14 | 3/2 | |
| Fe | Fe | Zn | Zn | −3 | 0 | 56 | 79 | 1/2 | |
| Fe | Fe | Zn | Zn | −2 | 0 | 45 | 79 | 0 | |
| Fe | Fe | Zn | Zn | −1 | 0 | 15 | 13 | 1/2 | |
| Fe | Fe | Fe | Pd | −3 | 19 | 0 | 7 | 3/2, 5/2 | |
| Fe | Fe | Fe | Pd | −2 | 0 | 2 | 6 | 0, 1, 2 | |
| Fe | Fe | Fe | Pd | −1 | 0 | 24 | 45 | 1/2 | |
| Fe | Fe | Pd | Pd | −3 | 0 | 16 | 13 | 1/2 | |
| Fe | Fe | Pd | Pd | −2 | 0 | 5 | 39 | 0, 1 | |
| Fe | Fe | Pd | Pd | −1 | 0 | 38 | 35 | 1/2 | |

[a] For systems with an odd number of d electrons, $M_{S0} = 1/2$; for even numbers, $M_{S0} = 0$. [b] As that found in synthetic clusters or proteins. Some data are from *P. furiosus* ferredoxin, which contains an Asp instead of one of the Cys residues.

**TABLE 2: Comparison of Computed and Experimental Metal−Ligand Bond Lengths (Å)**

| cluster | | | | | thiolate M−S | | sulfide M−$S_{short}$ | | sulfide M−$S_{long}$ | |
|---|---|---|---|---|---|---|---|---|---|---|
| M1 | M5 | M17 | M18 | $Q$ | exp | comp | exp | comp | exp | comp |
| Fe | Fe | Fe | Fe | −3 | 2.30[54] | 2.28 | 2.30[54] | 2.31 | 2.35[54] | 2.31 |
| Fe | Fe | Fe | Fe | −2 | 2.25[54] | 2.25 | 2.24[54] | 2.29 | 2.31[54] | 2.29 |
| Fe | Fe | Fe | Co | −3 | 2.27[55] | 2.29 | 2.26[55] | 2.30 | 2.26[55] | 2.30 |
| Fe | Fe | Fe | Ni | −3 | 2.28[55] | 2.30 | 2.28[55] | 2.30 | 2.28[55] | 2.30 |

***[CrFe$_3$S$_4$].*** The reduced state ($Q = -3$) of this cluster had two electronic configurations virtually degenerate; the configurations with the lowest possible $M_S$ value of 1/2 and the second lowest of 3/2 are separated by only 6 kJ/mol, which is well within the uncertainty of any computational method. In *P. furiosus* ferredoxin, this cluster type gives rise to an $S = 3/2$ ground state,[48] which is consistent with close-lying $M_S = 1/2$ and 3/2 states (both should occur with a small energy separation). The computed oxidized state ($Q = -2$) displays an $M_S$ value of 1, whereas experimentally, this cluster is X-band EPR silent,[48] indicating a non-Kramer's even spin state, consistent with the computational finding. The hyperoxidized state ($Q = -1$), which formally contains three trivalent and one divalent metal ion, is computed to be similar in behavior to the reduced state, that is, displaying close-lying configurations of the lowest $M_S$ quantum numbers.

***[Cr$_2$Fe$_2$S$_4$].*** Experimental data are not available for the disubstituted heterometallic clusters. However, they have been studied with the aim of understanding how further metal substitution beyond one metal might affect cluster geometries,

electronic structure, and properties. First, it is interesting to understand why other combinations of metals have not been chosen for the iron−sulfur clusters, including those with more heterometals. Second, in the process of designing new catalysts, we are, in principle, not limited to any subset of the combinatorial space of chemical modifications. Third, the disubstituted clusters provide a unique insight into electronic structure and spin coupling in these cluster types which cannot be obtained from simple monosubstituted clusters. For example, the presence of two heterometals will tend to force the remaining iron atoms to spin couple down, as seen later, providing a new basis for variation and tuning of the electronic structure.

In the [$Cr_2Fe_2S_4$] clusters, all ground states are obtained as fully antiferromagnetically coupled states with minimum $M_S$ values. However, in the two more oxidized clusters, the coupling is weaker, and the $M_{S0}$ and $M_{S0+1}$ configurations become pseudodegenerate.

***[MnFe$_3$S$_4$].*** The monosubstituted manganese cluster is interesting for its expected similarity with the native cluster, that is, preferring local high-spin sites. A fully antiferromagnetic coupling scheme is anticipated because of the close-lying d orbitals of Mn and Fe and thus the improved superexchange pathways. This behavior is clearly seen in the normally accessible redox states $Q = -3$ and $-2$, which have $M_{S0}$ configurations lowest in energy with substantial energy gaps (32 and 59 kJ/mol) to other configurations. This is also consistent with magnetic data of the corresponding cluster in *P. furiosus* ferredoxin, deduced to have an $S = 0$ ground state.[49] On the other hand, the hyperoxidized cluster exhibits an unusual degeneracy of the three configurations, suggesting that this complex exhibits spin-crossover tendencies.

***[Mn$_2$Fe$_2$S$_4$].*** The disubstituted Mn clusters have the same characteristics as the monosubstituted counterparts, with strong antiferromagnetic coupling and the hyperoxidized state being pseudodegenerate. This comparison illustrates the similarity of iron and manganese in defining the electronic structure. Both metals prefer high-spin local sites with strong coupling due to similar d orbital energy levels.

***[Fe$_4$S$_4$].*** The conventional all-iron clusters exhibit fully antiferromagnetic states, with comfortable gaps to the next configurations, in agreement with consensus.[2] However, in the listed experimental data, there is also the case of an $S = 3/2$, 1/2 quantum admixture[53] in the fully reduced state,[50] which is not observed here in the bare cluster. As this is not observed in general, it is reasonable to conclude that full antiferromagnetic coupling is observed in the isolated clusters, as obtained here, whereas perturbations caused by the protein can change this situation in specific cases such as the [$Fe_4S_4$] cluster in *P. furiosus* ferredoxin. This intrinsic preference of the clusters for full spin-down coupling is an interesting result in relation to the debate about what factors influence the accessibility of the $M_S = 3/2$ configuration in certain proteins.[2]

***[CoFe$_3$S$_4$].*** The cobalt clusters are interesting in having experimental data clearly indicating a change from incomplete antiferromagnetic coupling in the reduced cluster ($Q = -3$) to full antiferromagnetic coupling in the oxidized cluster ($Q = -2$).[49] The computed energies give a similar picture, with the $M_S = 1/2$ ground state for $Q = -2$ but a "triplet" ground state for $Q = -1$, both with comfortable separations (18 and 56 kJ/mol) to other configurations. This observation can be rationalized directly from the computations as discussed later, implying a $2Fe^{2.5}$ valence-delocalized $S = 9/2$ site spin-coupling with an $S = -7/2$ Co(II)/Fe(II) site in the reduced cluster or an $S = -9/2$ Co(III)/Fe(III) coupled to a 2Fe(II) $S = 8/2$ site in the oxidized cluster.

***[Co$_2$Fe$_2$S$_4$].*** In the same way as the monosubstituted cobalt clusters, the disubstituted clusters exhibit changes in coupling schemes depending on the oxidation state. The reduced state can be interpreted as a Co(II)/Co(II) $S = 6/2$ site coupling with the $2Fe^{2.5}$ $S = 9/2$ site, giving $S = 3/2$. In the oxidized state, the main configuration must be a $2Fe^{2.5}$ $S = 9/2$ site coupling with the Co(III)/Co(II) intermediate spin, valence-localized $S = -5/2$ state to give $S = 2$, as explained later.

***[NiFe$_3$S$_4$].*** Various $M_S$ configurations are closer in energy for the Ni clusters than those for the Mn clusters. An $S = 3/2$ state has been observed in the protein.[51] This observation is consistent with our finding of a lowest energy for $M_S = 3/2$, indicating an electronic structure with the $2Fe^{2.5}$ site spin-coupling to a Ni(II)/Fe(II) $S = 6/2$ site. However, other configurations are only 15 and 26 kJ/mol above. Similarly, in the oxidized state for which experimental data are not available, the computed ground state has $M_S = 1$, indicating that the electron has been removed from the Ni/Fe site; however, the spin densities indicate that all sites differ. Other configurations are only 13 and 19 kJ/mol above the $M_S = 1$ configuration.

***[Ni$_2$Fe$_2$S$_4$].*** The disubstituted nickel clusters also exhibit very close-lying states but with a tendency to favor full antiferromagnetic coupling. However, the energy gaps are within the uncertainty of the method in this case, and no conclusion can be drawn as to the exact spin of this cluster.

***[CuFe$_3$S$_4$].*** The reduced Cu cluster has an $S = 2$ ground state in the protein,[48] which is consistent with expected spin coupling of a Cu(II)/Fe(II) $S = 5/2$ site to the usual $2Fe^{2.5}$ $S = 9/2$ site. Computations give a similar result, with a good separation of 34 kJ/Mol from the $M_S = 2$ configuration to the $M_S = 1$ configuration. In the oxidized ($Q = -2$) cluster, the experiment was interpreted as fully antiferromagnetic coupling ($M_S = 1/2$), indicating an unusual equivalent Fe(II)/Fe(II) $S = 8/2$ site spin coupling to a Cu(III)/Fe(III) $S = 7/2$ site. This is the only case where our computations are not consistent with experiment, but all three configurations are close in energy, with the lowest-energy $M_S = 3/2$ configuration favored by only 14 kJ/mol.

***[Cu$_2$Fe$_2$S$_4$].*** These clusters again exhibit close-lying spin states with changing coupling schemes. The reduced state, computed to be comfortably $M_S = 1/2$, is directly explained as having coupled iron sites (one more oxidized than the other), with a total $S = 1/2$, spin-coupling to two equivalent Cu(II) sites. The oxidized state has all three configurations within 9 kJ/mol of each other, and no conclusion can be drawn, but an admixed state is anticipated. It is interesting to see that antiferromagnetic coupling is preferred even for the two irons left over when two copper ions take up the remaining sites, indicating that this is generally the preferred interaction for two high-spin metal ions.

***[ZnFe$_3$S$_4$].*** The Zn clusters serve a special role in the series by being redox-inactive and thus not contributing to any spin coupling within the clusters. On this background, it can be deduced that the [$ZnFe_3S_4$] clusters will resemble [$Fe_3S_4$] clusters in terms of spin coupling, that is, leaving one iron site uncoupled with a final spin corresponding to that site. In the reduced state, this corresponds to the observed $S = 5/2$, whereas in the oxidized state, it corresponds to $S = 2$.[52] Both of these observations are reproduced from the calculations. In the hyperoxidized state, all configurations are close in energy, and the same conclusion is no longer obvious.

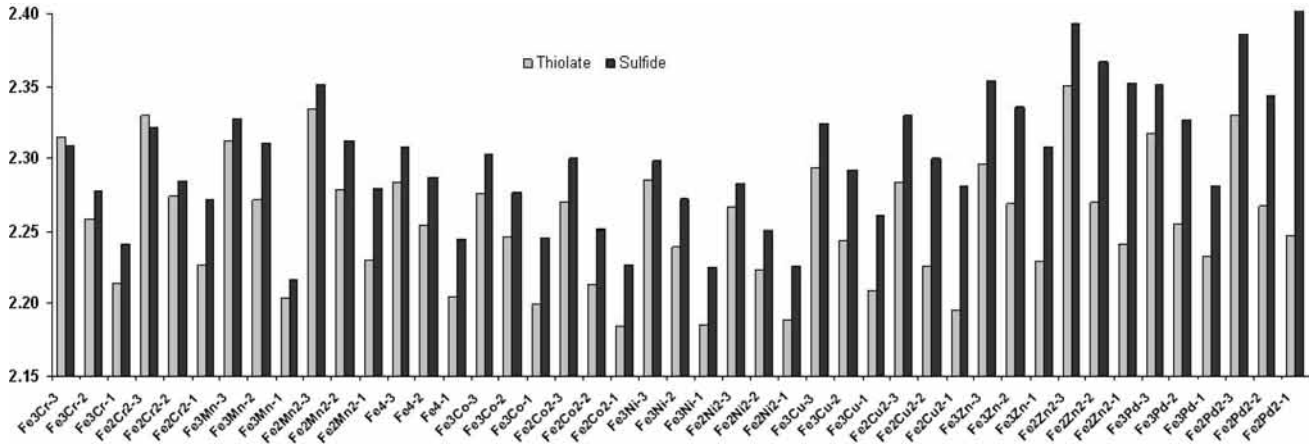


**Figure 3.** Average metal−thiolate and metal−sulfide bond lengths (Å) in computed clusters.

***[Zn$_2$Fe$_2$S$_4$].*** The dizinc clusters, although never studied experimentally, can be predicted to be similar to the [Fe$_2$S$_2$] iron−sulfur clusters in terms of spin coupling, that is, exhibiting full antiferromagnetic coupling. It is encouraging to see from the computations in Table 1 that this is indeed the case, with the reduced and oxidized clusters having $M_S$ values of 1/2 and 0, respectively, with significant energy gaps (56 and 45 kJ/mol) to the higher $M_S$ configurations. Thus, we can confidently predict the electronic structures of these clusters.

***[PdFe$_3$S$_4$].*** Finally, we turn to the Pd-containing clusters, which have been included due to the special use of Pd as a catalyst and the interesting comparison it makes to the other clusters, particularly by being a second-row transition metal. The clusters have spin couplings resembling the Ni clusters, and in most cases, the ground states are the same. The only exception is the oxidized [PdFe$_3$S$_4$] cluster, which however has all three configurations within only 6 kJ/mol and is thus indicated to be strongly quantum-admixed.

***[Pd$_2$Fe$_2$S$_4$].*** Fully spin-down coupled electronic configurations are found for all of these clusters, resembling the situation found for the [Ni$_2$Fe$_2$S$_4$] clusters.

**Geometries.** ***Comparison with Experimental Data.*** With the consistent and qualitatively correct assignment of the ground states of the clusters, we now compare the computed structural data with experimental geometries, where possible, to get an impression of the accuracy of the geometry optimizations. It is noteworthy that all geometry-optimized clusters represent stable cuboidal structures, in agreement with experimental data of synthesized models and heterometal-substituted cores in proteins, with the one exception being the Pd clusters, to be discussed later. Experimental and computed data are compared in Table 2 for reduced and oxidized model complexes.[54] We have concentrated on comparing the essential metal−sulfur bond lengths as these are quite sensitive to oxidation state and sometimes nature of the metal.

As seen from Table 2, the average iron−sulfur bond lengths are within 0.04 Å of experiment in both reduced and oxidized clusters. Including data for cobalt and nickel clusters in proteins does not change this general assessment. The overall mean absolute error (MAE) for all bonds is 0.024 Å, which is typical and expected for BP86-optimized geometries of metal clusters.

***Trends in Bond Lengths as a Function of Oxidation States.*** The equilibrium bond lengths for all clusters in their optimized ground states are discussed here and can be found in Supporting Information Table S5. For each cluster, all four metal−thiolate bond lengths are shown, whereas the average of the three metal−sulfide bonds is shown for each metal (12 bonds all together condensed into 4 average bond lengths). Due to the high accuracy accounted for above, these results constitute a useful database of metal−sulfur bond lengths and contain information about the bonding and electronic structure which is supplemented by population analysis (see later). Table S5 can thus be used as a guideline for determining metal−sulfur bond lengths in this general class of heterometallic clusters.

Although many metal ions and several oxidation states are described, the clusters do share some common features. Most importantly, there is a clear shortening of bond lengths in higher oxidation states which may be used to refine and understand experimental structures and which is also observed experimentally in high-resolution structures of small model complexes.[54] Figure 3 shows the averages over all metal−sulfide and metal−thiolate bond lengths in the clusters, for each cluster in each oxidation state.

It is apparent from Figure 3 that the average lengths of both metal−thiolate and metal−sulfide bonds decrease systematically with increasing oxidation state. There is a tendency for the metal−thiolate bonds to be more sensitive than the metal−sulfide bonds, with typical shortenings of 0.05 Å per oxidation state for the former, and 0.02−0.03 Å per oxidation state for the latter. These effects reflect electronic repulsion within the clusters and therefore also the sensitivity of metal−thiolate bonds to changes in the environment, as shown in earlier work.[20]

***Trends in Bond Lengths as a Function of Heterometal.*** From the bond lengths in Table S5, it can also be deduced that certain geometric features are very sensitive to the type of metals situated in the clusters. The larger effects are seen in the reduced clusters. As expected, the iron−sulfur bonds change the least when heterometals are introduced in the clusters, and the largest changes of ∼0.05 and 0.08 Å in metal−thiolate and metal−sulfide bonds, respectively, occur upon substitution of two Fe with two Zn.

Much larger effects are seen directly in the heterometal−sulfur bonds, both for the metal−thiolate bonds (2.23−2.37 Å) and, in particular, for metal−sulfide bonds (2.28−2.53 Å). For metal−thiolate bonds, the order of increasing bond lengths is [NiFe$_3$S$_4$] ∼ [Ni$_2$Fe$_2$S$_4$] ∼ [CoFe$_3$S$_4$] ∼ [Co$_2$Fe$_2$S$_4$] < [CuFe$_3$S$_4$] ∼ [Cu$_2$Fe$_2$S$_4$] < [ZnFe$_3$S$_4$] < [Cr$_2$Fe$_2$S$_4$] < [Mn$_2$Fe$_2$S$_4$] < [MnFe$_3$S$_4$] < [CrFe$_3$S$_4$] < [Zn$_2$Fe$_2$S$_4$] ∼ [PdFe$_3$S$_4$] ∼ [Pd$_2$Fe$_2$S$_4$]. For sulfide bonds, the order is [Ni$_2$Fe$_2$S$_4$] < [Co$_2$Fe$_2$S$_4$] ∼ [CoFe$_3$S$_4$] < [NiFe$_3$S$_4$] ∼ [CrFe$_3$S$_4$] ∼ [Cr$_2$Fe$_2$S$_4$] < [MnFe$_3$S$_4$] < [Mn$_2$Fe$_2$S$_4$] < [Cu$_2$Fe$_2$S$_4$] < [CuFe$_3$S$_4$] < [ZnFe$_3$S$_4$] < [Zn$_2$Fe$_2$S$_4$] < [Pd$_2$Fe$_2$S$_4$] < [PdFe$_3$S$_4$]. These two series are very similar, with the exception of Cu bonds.

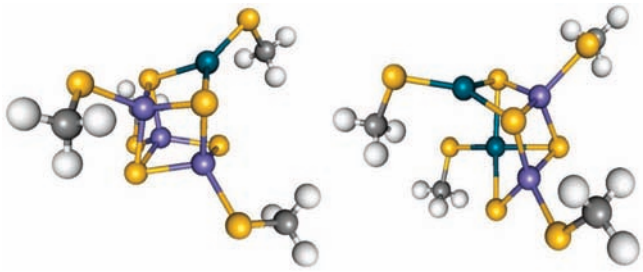

**Figure 4.** Geometric distortions in optimized structures of $[PdFe_3S_4]^{2+}$ (left) and $[Pd_2Fe_2S_4]^{2+}$ (right). Hydrogens are shown in white, carbons in gray, sulfurs in yellow, irons in blue, and palladiums in azur.

In the oxidized cluster, the Fe−S bonds are 2.25−2.28 Å for metal−thiolate bonds and 2.22−2.32 Å for metal−sulfide bonds. The heterometal−thiolate bonds range from 2.18 (with two cobalt) to 2.32 Å (with one or two Pd). Also in this oxidation state, the most significant changes occur in the heterometal−sulfide bond lengths, ranging from 2.23 Å in $[CrFe_3S_4]$ and $[Co_2Fe_2S_4]$, to 2.44 Å in $[ZnFe_3S_4]$ and $[Zn_2Fe_2S_4]$ and 2.47 and 2.64 Å in $[Pd_2Fe_2S_4]$ and $[PdFe_3S_4]$, the latter being due to Pd being larger and to the formation of unprecedented geometries in these clusters, as depicted in Figure 4. The tendency of Pd(II) to form square-planar complexes and the relative destabilization of the $d_{x^2-y^2}$ orbital is very strong; with one Pd present, a trigonal distortion of the tetrahedral geometry is preferred, causing the cuboidal structure to distort, as shown in Figure 4. With two Pd atoms present, one is trigonally distorted and one is almost square-planar. Due to Jahn−Teller distortion in the $D_{3h}$ geometry, but not that in the $D_{4h}$ geometry, and because the third sulfide will remain positioned in the cluster weakly coordinating to Pd, the actual geometry of Pd is not perfectly trigonal. However, when two Pd atoms are present, the third sulfide moves far toward forming a tetragonal Pd in one site and a trigonal Pd in the other side. This effect is most extreme in the oxidized cluster.

**Reduction Potentials.** Proteins strongly affect the reduction potential of any cluster and can tune it dramatically by *at least* half a volt.[26] However, the intrinsic propensity of a cluster to allow certain redox states is very much defining the function, whereas the protein effect can be thought of as a perturbation to this zero-order effect. For fundamental understanding and for subsequent design purposes, we are interested in the latter, intrinsic contributions to the reduction potentials, and not the somewhat random effects of individual proteins. In a later step of an ideal design process, it is quite feasible to tune the intrinsic potentials by specific apoprotein design strategies, including site-directed mutagenesis of amino acid ligands close to the modified cluster.

Expected errors of ionization energies are ∼30 kJ/mol for BP86 and B3LYP, based on small first-row transition-metal oxides and hydrides.[10] In addition, the use of the experimentally determined standard potential of the hydrogen electrode as a reference renders only the relative reduction potentials meaningful. However, the relative potentials are in fact accurate to within ∼10 kJ/mol, owing to cancelation of errors in reference potentials, solvation models, and so forth. Still, it is important to provide some account of screening effects for both redox states, and Cosmo is an excellent model for this purpose.

The computed absolute reduction potentials $E^0$, measured in volts, are compiled in Table 3 and shown in Figure 5; a large positive value of $-E^0$ means a large negative value of $E^0$, meaning harder to reduce. Due to the above-mentioned extrinsic effects, we will be concerned only with the relative shifts here.

**TABLE 3: Computed Reduction Potentials (V) and Inner-Sphere Self-Exchange Reorganization Energies (kJ/mol)**

| cluster | | | | | reaction energy | | | |
|---|---|---|---|---|---|---|---|---|
| M1 | M5 | M17 | M18 | $Q$ | $-E^0$ (V) | $\lambda_{ox}$ (kJ/mol) | $\lambda_{RED}$ (kJ/mol) | $\lambda_{TOT}$ (kJ/mol) |
| Fe | Fe | Fe | Cr | −3 | 1.74 | 37 | 11 | 48 |
| Fe | Fe | Fe | Cr | −2 | 0.65 | 23 | 21 | 44 |
| Fe | Fe | Fe | Cr | −1 | | | | |
| Fe | Fe | Cr | Cr | −3 | 1.35 | 31 | 29 | 60 |
| Fe | Fe | Cr | Cr | −2 | 0.64 | 16 | 20 | 37 |
| Fe | Fe | Cr | Cr | −1 | | | | |
| Fe | Fe | Fe | Mn | −3 | 1.39 | 36 | 44 | 80 |
| Fe | Fe | Fe | Mn | −2 | 0.34 | 8 | 64 | 73 |
| Fe | Fe | Fe | Mn | −1 | | | | |
| Fe | Fe | Mn | Mn | −3 | 0.97 | 23 | 86 | 109 |
| Fe | Fe | Mn | Mn | −2 | 0.59 | 28 | 24 | 51 |
| Fe | Fe | Mn | Mn | −1 | | | | |
| Fe | Fe | Fe | Fe | −3 | 1.74 | 25 | 23 | 47 |
| Fe | Fe | Fe | Fe | −2 | 0.52 | 27 | 20 | 46 |
| Fe | Fe | Fe | Fe | −1 | | | | |
| Fe | Fe | Fe | Co | −3 | 1.59 | 16 | 40 | 57 |
| Fe | Fe | Fe | Co | −2 | 0.74 | 17 | 16 | 33 |
| Fe | Fe | Fe | Co | −1 | | | | |
| Fe | Fe | Co | Co | −3 | 1.30 | 36 | 41 | 77 |
| Fe | Fe | Co | Co | −2 | 0.96 | 40 | 21 | 61 |
| Fe | Fe | Co | Co | −1 | | | | |
| Fe | Fe | Fe | Ni | −3 | 1.37 | 20 | 24 | 44 |
| Fe | Fe | Fe | Ni | −2 | 0.58 | 10 | 47 | 57 |
| Fe | Fe | Fe | Ni | −1 | | | | |
| Fe | Fe | Ni | Ni | −3 | 1.34 | 21 | 24 | 45 |
| Fe | Fe | Ni | Ni | −2 | 0.68 | 20 | 15 | 35 |
| Fe | Fe | Ni | Ni | −1 | | | | |
| Fe | Fe | Fe | Cu | −3 | 1.14 | 30 | 23 | 53 |
| Fe | Fe | Fe | Cu | −2 | 0.46 | 22 | 18 | 40 |
| Fe | Fe | Fe | Cu | −1 | | | | |
| Fe | Fe | Cu | Cu | −3 | 1.02 | 39 | 36 | 75 |
| Fe | Fe | Cu | Cu | −2 | 0.26 | 7 | 7 | 13 |
| Fe | Fe | Cu | Cu | −1 | | | | |
| Fe | Fe | Fe | Zn | −3 | 1.49 | 15 | 16 | 31 |
| Fe | Fe | Fe | Zn | −2 | 0.32 | 24 | 22 | 46 |
| Fe | Fe | Fe | Zn | −1 | | | | |
| Fe | Fe | Zn | Zn | −3 | 1.53 | 21 | 18 | 39 |
| Fe | Fe | Zn | Zn | −2 | −0.17 | 18 | 36 | 54 |
| Fe | Fe | Zn | Zn | −1 | | | | |
| Fe | Fe | Fe | Pd | −3 | 1.15 | 66 | 59 | 125 |
| Fe | Fe | Fe | Pd | −2 | 0.68 | 45 | 27 | 72 |
| Fe | Fe | Fe | Pd | −1 | | | | |
| Fe | Fe | Pd | Pd | −3 | 1.49 | 57 | −1 | 56 |
| Fe | Fe | Pd | Pd | −2 | 0.40 | 12 | 13 | 25 |
| Fe | Fe | Pd | Pd | −1 | | | | |

The relative shifts in cluster potentials for the biologically relevant $Q = -3/-2$ redox equilibrium have been calculated using the all-iron clusters as the reference and compared to experimental shifts in reduction potentials of the clusters in *P. furiosus* ferredoxin,[4] as depicted in Figure 6. A further advantage of computational chemistry is that, experimentally, the clusters lose their heterometal above −0.1 V,[4] whereas in silico, these potentials can be studied more accurately in the optimized clusters without lower limits.

*P. furiosus* ferredoxin contains an Asp most likely coordinating to the heterometal, whereas the clusters and other proteins have four cysteines coordinating the metals. However, the effect of the Asp versus Cys has been well-accounted for, with a shift in reduction potential of 0.06 V.[21,56] Thus, we use the *P. furiosus* ferredoxin data as they are available for more clusters and thus provide a better statistic data set. Agreement between computed and experimental shifts is very good, with a mean absolute error

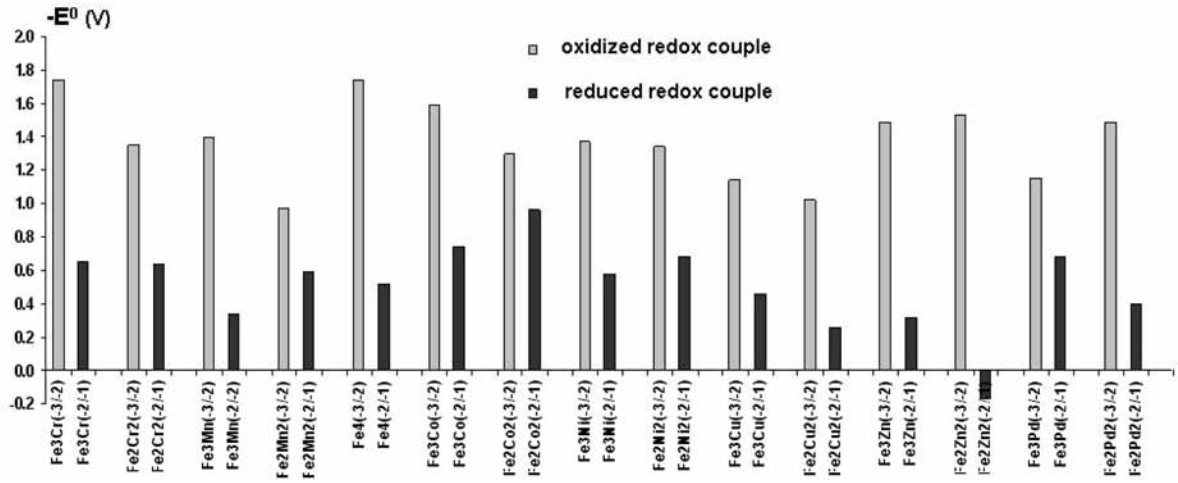


**Figure 5.** Computed absolute reduction potentials of iron−sulfur clusters.

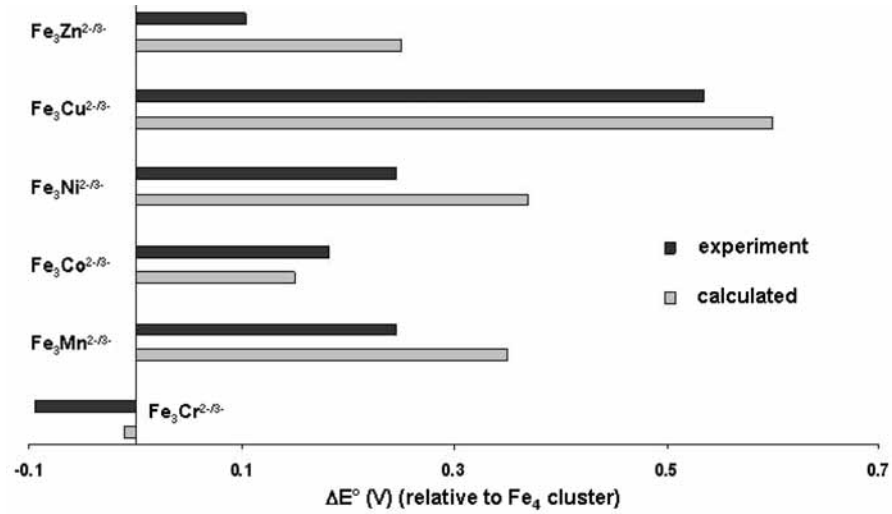


**Figure 6.** Computed and experimental shifts in reduction potentials with $Fe_4$ cluster as reference. MAE = 0.093 V.

of 0.093 V for $[CrFe_3S_4]$, $[MnFe_3S_4]$, $[CoFe_3S_4]$, $[NiFe_3S_4]$, $[CuFe_3S_4]$, and $[ZnFe_3S_4]$ relative to $[Fe_4S_4]$.

As is apparent from the potentials in Figure 5, the $[Fe_4S_4]$ cluster has the most negative reduction potential together with $[CrFe_3S_4]$ for the oxidized state, meaning that these two are hardest to reduce. On the other hand, the second potential is intermediate in the series. This implies that for the biologically relevant redox couple, any heterometal substitution except Cr will make the cluster easier to reduce. The reason why the native cluster is at an extreme value is probably due to the need for reversibility in the redox reaction, an effect further strengthened in *P. furiosus* ferredoxin by using Asp to selectively stabilize redox states by changing the coordination mode.[21]

The experimental trend, which is more or less constant among proteins, was rationalized from electron-withdrawing properties of the heterometals, and a trend of Cu > Ni/Mn > Co > Zn > Fe > Cr was found.[57] In our case, Fe ∼ Cr, and the computations are in quite good qualitative agreement with this conclusion, as seen in Figure 6. One may then suggest that the iron−sulfur cluster has been evolved to have reasonably hard redox-active metal ions, of which Cr or Fe do well. However, iron is much more abundant and easier to handle in the general "infrastructure" or physiology of early organisms. As we shall see, Cr is also equally competitive with Fe in terms of having low reorganization energies in these clusters.

**Reorganization Energies.** Iron−sulfur clusters are known to have many biological functions, but one of the most important is to transfer electrons, as in the case of ferredoxins. In our computational effort to understand molecular evolution and design alternative molecular systems, we have to describe the relevant reactivity parameters and compare them among molecular alternatives to elucidate why nature is using one alternative over another. The most efficient electron-transport systems are those that have been evolved to maximize the electron-transfer rate while at the same time providing an optimal redox potential for the problem at hand. Due to restrictions in the availability of redox-active clusters, this has been a serious selection pressure in molecular evolution of organisms. In turns out that only three general classes of metal-containing electron-transfer clusters are used by nature, namely, cytochromes, blue copper proteins, and iron−sulfur clusters. Therefore, what is so special about these clusters?

The semiclassical Marcus eq 2 serves as a useful framework for these investigations[58]

$$k_{ET} = \frac{H_{DA}^2}{\hbar\sqrt{\lambda RT/\pi}} \exp\left(-\frac{(E^0+\lambda)^2}{4\lambda RT}\right) \qquad (2)$$

Using this equation, the rate of electron transfer ($k_{ET}$) can be described as depending on three parameters: the electronic coupling element ($H_{DA}^2$), the redox potential ($E^0$), and the reorganization energy ($\lambda$). These parameters can again be divided into intrinsic parts related to the metal site itself (including the first coordination sphere) and extrinsic parts due to the protein

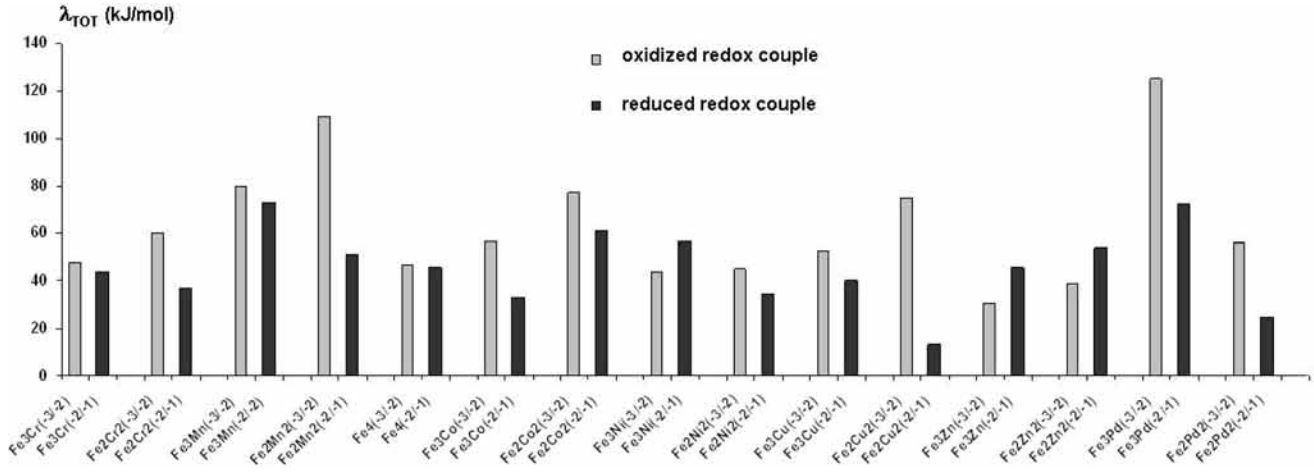


**Figure 7.** Computed self-exchange inner-sphere reorganization energies of modified [$Fe_4S_4$] clusters.

(second coordination sphere and beyond). Both parts have been optimized by evolution.

The absolute magnitude of the coupling element can be maximized by enforcing a large overlap between donor and acceptor orbitals. We have recently suggested[20] that electron-rich clusters such as iron−sulfur clusters can better extend their electron densities to maximize the overlap of frontier orbitals involved in electron transfer, thereby maximizing $H_{AD}$ for both oxidation and reduction reactions.

Focus here will thus be on the two parameters which govern the exponential rate behavior and thus possess the largest potential for tuning, $\lambda$ and $E^0$. For the purpose of understanding the choice of metal sites themselves, we are concerned with the intrinsic parts of these parameters, which do not depend on the detailed structures of individual proteins. Thus, the cluster reduction potential and the self-exchange inner-sphere reorganization energy ($\lambda_I$) have been computed, similar to what has been done for native iron−sulfur clusters,[13,20] blue-copper proteins, and cytochromes.[27,28]

The $\lambda_I$ is defined as the total energy required to distort the oxidized ($\lambda_{OX}$) and reduced ($\lambda_{RED}$) states into each other during a self-exchange electron-transfer reaction of the metal site. This energy is per definition the Marcus inner-sphere self-exchange reorganization and can be directly calculated by electron structure methods.[27] It directly quantifies the ability of a metal complex to engage in reversible electron-transfer processes. The results are shown in Figure 7.

Analyzing the results in Figure 7, a stark contrast to smaller iron−sulfur clusters[13,20] is seen in the low reorganization energies across the series. The $Fe^{II}/Fe^{III}$ redox pair is superior for reversible electron transport in both weak-field (HS) tetrahedral and strong-field (LS) octahedral ligand fields because a bonding d orbital becomes occupied upon reduction, whereas other metals in the biologically relevant redox regime need to occupy an antibonding d orbital when reduced. Interestingly, the strong field is observed in the cytochromes, whereas the weak field is observed in the iron−sulfur clusters. Furthermore, it is apparent from our data that whereas any metal substitution in [$Fe_2S_2$] clusters severely increases the reorganization energy by typically 50−100 kJ/mol,[13] in the [$Fe_4S_4$] clusters, reorganization energies remain low in most clusters, except Mn and Pd, the latter due to the severe distortion effects discussed earlier. In the $Pd_2$ cluster, the distortions are present in all states, and thus, the reorganization energy remains low.

The reason for the low reorganization energies can be analyzed to be due to the continued presence of a redox-active Fe(II)/Fe(III) site. This site is however *not* locally reduced to obey the rule[13] of occupying only bonding-type d orbitals during the redox reaction. Instead, the valence delocalization and multiconfigurational nature of the clusters ensures that the reducing electron is distributed well over the cluster, depending on each cluster's preference, as we will discuss in more detail in the next section. In other words, the electronic structure of the [$Fe_4S_4$] clusters implies, among other things, a large robustness toward "pollution" with other metals. This observation may have several biological implications; for example, it may indicate that heterometals are more commonly found in the large iron−sulfur clusters and that these clusters take part in metal storage and transport as has been hypothesized.[4]

**Analysis of Electronic Structures.** To obtain a better understanding of the detailed bonding and electronic structure in the various heterometallic clusters, we have performed Mulliken population analysis of all geometry-optimized clusters and compiled the atomic excess spin and charges for all metals. These results can be found in Table 4. In the following, we will discuss each cluster type separately. In general, the sulfur atoms take up a substantial part of the total spin, typically 0.2 au per atom, which is in accord with generally observed spin delocalization effects in transition-metal systems. Another general observation is that metal charges decrease upon cluster oxidation. This is due to charge delocalization in all clusters (that ligands contain a major part of the unpaired electron density) and to the fact that bonds shorten considerably in the oxidized states, so that more electron density is being assigned to the metals in the population analysis. It is important not to forget that covalency effects play a major role in the electronic structures, but in the analysis, we will try to keep these out in order to provide a simpler and more chemically appealing atomic-based analysis of formal oxidation states.

***[CrFe$_3$S$_4$].*** The reduced state of this cluster ($Q = -3$) can be described formally as either a valence-delocalized $2Fe^{2.5}$ site (spin densities 3.18/3.19) with $S = +9/2$, antiferromagnetically coupled to the Cr(II)/Fe(II) site (spin densities −2.97/−2.97) with $S = -8/2$, or as a 2Fe(II) site with $S = 8/2$ and a Cr(III)/Fe(II) site with $S = -7/2$, which would also lead to complete antiferromagnetic coupling. We have already discussed the only 6 kJ/mol separation of the two lowest $M_S$ values, corresponding to flipping one spin (there are several ways of doing this, only one of which is realized in the broken-symmetry approach). The real ground state is most likely a multiconfigurational state with contributions from several intermediate $M_S = 0$ and 3/2 configurations. In the reduced cluster, the spin density on Cr

**TABLE 4: Metal Spin and Charges of Optimized Cluster Ground States**

| cluster | | | | | charges | | | | spin | | | |
|---|---|---|---|---|---|---|---|---|---|---|---|---|
| M1 | M5 | M17 | M18 | *Q* | M1 | M5 | M17 | M18 | M1 | M5 | M17 | M18 |
| Fe | Fe | Fe | Cr | −3 | 0.22 | 0.18 | 0.21 | 0.00 | 3.18 | −2.97 | 3.19 | −2.97 |
| Fe | Fe | Fe | Cr | −2 | 0.17 | 0.17 | 0.09 | −0.21 | 3.07 | 3.09 | −2.75 | −1.93 |
| Fe | Fe | Fe | Cr | −1 | 0.01 | 0.01 | 0.02 | −0.27 | 2.36 | 2.43 | −2.54 | −1.66 |
| Fe | Fe | Cr | Cr | −3 | 0.27 | 0.28 | 0.05 | 0.05 | 3.25 | 3.27 | −3.32 | −3.33 |
| Fe | Fe | Cr | Cr | −2 | 0.13 | 0.12 | −0.02 | −0.04 | 2.57 | 2.59 | −3.06 | −3.03 |
| Fe | Fe | Cr | Cr | −1 | 0.07 | 0.08 | −0.16 | −0.13 | 2.48 | 2.57 | −2.56 | −2.65 |
| Fe | Fe | Fe | Mn | −3 | 0.18 | 0.18 | 0.18 | 0.25 | 3.13 | −3.33 | −3.34 | 4.11 |
| Fe | Fe | Fe | Mn | −2 | 0.09 | 0.09 | 0.11 | 0.22 | −3.12 | −3.16 | 3.32 | 4.18 |
| Fe | Fe | Fe | Mn | −1 | −0.08 | −0.04 | −0.16 | −0.01 | 2.00 | −2.50 | −0.18 | 2.78 |
| Fe | Mn | Fe | Mn | −3 | 0.19 | 0.28 | 0.19 | 0.28 | −3.39 | 4.30 | −3.40 | 4.32 |
| Fe | Mn | Fe | Mn | −2 | 0.13 | 0.15 | 0.13 | 0.14 | −3.28 | 3.80 | −3.29 | 3.78 |
| Fe | Mn | Fe | Mn | −1 | −0.02 | 0.06 | −0.03 | 0.08 | −2.65 | 3.50 | −2.65 | 3.57 |
| Fe | Fe | Fe | Fe | −3 | 0.17 | 0.15 | 0.16 | 0.18 | 3.29 | −2.99 | −2.99 | 3.32 |
| Fe | Fe | Fe | Fe | −2 | 0.09 | 0.09 | 0.09 | 0.09 | 3.10 | 3.13 | −3.10 | −3.10 |
| Fe | Fe | Fe | Fe | −1 | 0.02 | 0.02 | −0.07 | −0.07 | 2.87 | 2.87 | −2.41 | −2.41 |
| Fe | Fe | Fe | Co | −3 | 0.18 | 0.18 | 0.16 | 0.12 | 3.30 | 3.32 | −3.14 | −1.80 |
| Fe | Fe | Fe | Co | −2 | 0.09 | 0.08 | 0.09 | 0.05 | 3.06 | 3.08 | −3.16 | −1.90 |
| Fe | Fe | Fe | Co | −1 | −0.05 | −0.04 | 0.03 | −0.04 | 2.55 | 2.61 | −3.02 | −1.76 |
| Fe | Co | Fe | Co | −3 | 0.17 | 0.13 | 0.18 | 0.12 | 3.31 | −1.93 | 3.34 | −1.97 |
| Fe | Co | Fe | Co | −2 | 0.07 | −0.02 | 0.08 | −0.06 | 2.93 | −1.30 | 2.97 | −0.82 |
| Fe | Co | Fe | Co | −1 | −0.06 | −0.11 | 0.00 | −0.06 | −2.56 | −1.10 | 2.87 | 1.57 |
| Fe | Fe | Fe | Ni | −3 | 0.14 | 0.18 | 0.18 | 0.11 | −3.22 | 3.33 | 3.32 | −0.68 |
| Fe | Fe | Fe | Ni | −2 | 0.09 | 0.00 | 0.12 | 0.04 | −3.12 | 2.72 | 3.23 | −0.76 |
| Fe | Fe | Fe | Ni | −1 | −0.05 | −0.19 | 0.02 | −0.03 | −2.60 | −0.54 | 2.93 | 0.67 |
| Fe | Ni | Fe | Ni | −3 | 0.16 | 0.11 | 0.16 | −0.24 | −3.33 | 0.92 | 3.32 | −0.24 |
| Fe | Ni | Fe | Ni | −2 | 0.10 | 0.03 | −0.02 | 0.00 | −3.20 | 0.70 | 2.56 | −0.15 |
| Fe | Ni | Fe | Ni | −1 | −0.11 | −0.08 | 0.01 | −0.07 | −2.13 | 0.09 | 2.94 | −0.08 |
| Fe | Fe | Fe | Cu | −3 | 0.19 | 0.14 | 0.19 | 0.05 | 3.36 | −3.33 | 3.38 | 0.05 |
| Fe | Fe | Fe | Cu | −2 | 0.10 | 0.00 | 0.07 | −0.03 | 3.13 | 2.63 | −3.15 | 0.02 |
| Fe | Fe | Fe | Cu | −1 | −0.11 | −0.08 | 0.01 | −0.09 | 2.24 | 2.37 | −2.97 | 0.02 |
| Fe | Fe | Cu | Cu | −3 | 0.20 | 0.15 | 0.03 | 0.03 | 3.46 | −3.36 | 0.17 | 0.18 |
| Fe | Fe | Cu | Cu | −2 | 0.04 | −0.15 | −0.05 | −0.02 | 2.76 | 0.40 | −0.01 | 0.04 |
| Fe | Fe | Cu | Cu | −1 | −0.10 | −0.08 | −0.08 | −0.09 | 2.27 | 2.35 | −0.03 | −0.08 |
| Fe | Fe | Fe | Zn | −3 | 0.22 | 0.16 | 0.23 | 0.39 | 3.50 | −2.99 | 3.50 | 0.00 |
| Fe | Fe | Fe | Zn | −2 | 0.15 | 0.08 | 0.14 | 0.36 | 3.37 | −3.31 | 3.39 | 0.00 |
| Fe | Fe | Fe | Zn | −1 | 0.02 | 0.01 | −0.04 | 0.34 | 3.02 | −3.15 | 2.74 | 0.01 |
| Fe | Fe | Zn | Zn | −3 | 0.23 | 0.23 | 0.39 | 0.39 | −3.21 | 3.65 | 0.00 | 0.00 |
| Fe | Fe | Zn | Zn | −2 | 0.13 | 0.12 | 0.36 | 0.36 | −3.52 | 3.53 | 0.00 | 0.00 |
| Fe | Fe | Zn | Zn | −1 | −0.10 | 0.06 | 0.34 | 0.32 | −2.80 | 3.41 | 0.00 | −0.01 |
| Fe | Fe | Fe | Pd | −3 | 0.17 | 0.15 | 0.17 | −0.11 | 3.25 | −3.33 | 3.25 | −0.31 |
| Fe | Fe | Fe | Pd | −2 | −0.14 | 0.12 | 0.01 | −0.17 | 1.18 | −3.17 | 2.47 | −0.18 |
| Fe | Fe | Fe | Pd | −1 | 0.00 | −0.15 | −0.10 | −0.04 | −2.91 | 2.08 | 2.32 | −0.23 |
| Fe | Fe | Pd | Pd | −3 | 0.16 | 0.18 | −0.21 | −0.06 | 3.33 | −3.42 | −0.24 | −0.13 |
| Fe | Fe | Pd | Pd | −2 | −0.02 | −0.02 | −0.15 | −0.15 | 2.30 | −2.77 | 0.28 | −0.04 |
| Fe | Fe | Pd | Pd | −1 | −0.08 | −0.20 | −0.10 | −0.13 | 2.46 | −2.08 | 0.16 | 0.04 |

has changed by 1.04, indicating that Cr goes from Cr(III) to Cr(II), consistent with the Cr(III)/Fe(II) description of the reduced cluster. This is also consistent with a −0.21 charge on Cr, knowing that atomic charges become delocalized in electronic structures to be much closer to zero than formal charges of atomic ions.

***[Cr$_2$Fe$_2$S$_4$].*** In the reduced state, this cluster was clearly antiferromagnetically coupled as judged from the energies in Table 1, corresponding to a valence-delocalized $2Fe^{2.5}$ site ($S = 9/2$) and a 2Cr(II) site ($S = -8/2$). This structure is confirmed by equivalent spin densities of 3.25/3.27 for iron and −3.32/−3.33 for Cr. In the two more oxidized clusters, where coupling is weak as judged from the energies, both sites get partly oxidized (multiconfigurational description with 2Fe(III) + 2Cr(II) as one configuration and $2Fe^{2.5} + 2Cr^{2.5}$ as the other configuration), as seen in the spin densities. However in the hyperoxidized state, none of the metal ions are equivalent, indicating that several configurations are involved.

***[MnFe$_3$S$_4$].*** The fully antiferromagnetic coupling scheme is expected for Mn and clearly observed from the energies in the $Q = -3$ and −2 redox states, in agreement with experiment.[49] When we now analyze the electronic structure, we see that two irons are equivalent and have smaller spin density than the third iron, indicating that they form a $2Fe^{2.5}$ site coupled to an Fe(II)/Mn(II) site, in good agreement with relative spin densities (3.13/4.11). In the oxidized state, the electron is taken from the iron moiety, not affecting Mn. On the other hand, the hyperoxidized cluster exhibits an unusual degeneracy of the three configurations and has a higher $M_S$ quantum number.

***[Mn$_2$Fe$_2$S$_4$].*** As was the case with the dichromium cluster, the reduced form of this strongly coupled cluster consists of an iron and a heterometal site, each with equivalent ions. Spin densities of 4.30/4.32 for Mn and −3.39/−3.40 for Fe are fully consistent with a $2Fe^{2.5} + 2Mn(II)$ description. In the oxidized state, the Mn centers change spin density by ∼1/2 each, indicating that the electron is taken from them, giving a $2Fe^{2.5} + 2Mn^{2.5}$ ground state.

***[Fe$_4$S$_4$].*** The all-iron clusters exhibit fully antiferromagnetic states, with comfortable gaps to the next configurations, in agreement with what is usually found experimentally.[2] The

electronic structure can be described as a $2Fe^{2.5}$ + 2Fe(II) reduced ground state (spin densities of 3.29/3.32 and −2.99/−2.99, respectively). Upon oxidation, a fully symmetric, coupled $2Fe^{2.5}$ + $2Fe^{2.5}$ state is formed, with spin densities of 3.10, 3.13, −3.10, and −3.10. The hyperoxidized state then contains one electron less in one of these sites, giving rise to spin densities of 2.87, 2.87, −2.41, and −2.41, implying a $2Fe^{2.5}$ + 2Fe(III) state. Thus, the present computations provide a detailed account of the electronic structure that is consistent with what has been deduced from Mossbauer data and broken-symmetry calculations for the all-iron cluster[34] and which we now use also to study heterometallic clusters.

***[$CoFe_3S_4$].*** As mentioned earlier, the experimental data for this cluster indicate a change from incomplete antiferromagnetic coupling in the reduced cluster to full antiferromagnetic coupling in the oxidized cluster.[49] The $M_S = 1$ value is fully consistent with our computed energies in Table 1 and can be explained as due to a $2Fe^{2.5}$ $S = 9/2$ site (spin 3.30/3.32) coupling to a Co(II)/Fe(II) site with $S = -7/2$. This state has spin −3.14 for Fe, smaller than that for the more ferric sites, and −1.80 for Co. The oxidized state couples instead an $S = -9/2$ Co(III)/Fe(III) to a 2Fe(II) $S = 8/2$ site, as judged from most of the spin density taken from the $2Fe^{2.5}$ moiety.

***[$Co_2Fe_2S_4$].*** This cluster can be rationalized as having a reduced state with mainly a Co(II)/Co(II) $S = 6/2$ site coupling with the usual $2Fe^{2.5}$ $S = 9/2$ site, giving $S = 3/2$. In the oxidized state, the main configuration is a $2Fe^{2.5}$ $S = 9/2$ site coupling to the valence-localized intermediate spin Co(III)/Co(II) $S = -5/2$ state to give $S = 2$ (if the cobalt center had been high-spin, it would have given rise to an $S = 1$ ground state).

***[$NiFe_3S_4$].*** Both our computed state and experimental data[51] indicate an $S = 3/2$ state. Spin densities in Table 4 indicate a ground state described as a $2Fe^{2.5}$ site (3.33/3.32) spin-coupling to a Ni(II)/Fe(II) $S = 6/2$ site (−0.68/−3.22). The oxidized state has a computed ground state with $M_S = 1$, arising from a multiconfigurational state with no equivalent metal ions. The most important configurations would correspond to forms of Fe(II),Fe(III),Fe(III),Ni(II).

***[$Ni_2Fe_2S_4$].*** This cluster has an unusual electronic structure, which can be interpreted as the strong presence of Ni(I). The irons could have formed the usual $2Fe^{2.5}$ site but are antiferromagnetically coupled, in contrast to what has been seen in the other diheterometallic clusters. The two irons are equivalent but of opposite spin, whereas the Ni sites are inequivalent. The only two configurations which can explain this are localized Fe(III),Fe(III),Ni(I),Ni(II) and Fe(II),Fe(II),Ni(II),Ni(III). Due to the negative charge on Ni18 and its very low spin density, it seems clear that this Ni is Ni(I), consistent with the first of these two configurations. Having both a Ni(I) and a Ni(II) atom in such a cluster is an interesting situation which may lend hope to the ability of clusters like this one to activate hydrogen.

***[$CuFe_3S_4$].*** The $S = 2$ ground state of the reduced cluster[48] is consistent with a Cu(II)/Fe(II) $S = 5/2$ site coupling to the usual $2Fe^{2.5}$ $S = 9/2$ site. Computations are consistent with this result (and several other Cu(II) configurations); knowing that spin densities on metals are significantly smaller than a formal atomic ion state would imply being due to spin polarization.[15] In all redox states, the Cu remains inactive (the changes in charges can be rationalized from the decreasing bond lengths upon oxidation). The assignment becomes clearer in the oxidized ($Q = -2$) cluster, with experiment indicating $M_S = 1/2$, which can only be explained as an Fe(II)/Fe(II) $S = 8/2$ site coupling to a Cu(III)/Fe(III) $S = 7/2$ site. As mentioned earlier, this is the only case where our computations are not consistent with experiment, although all three $M_S$ configurations are close in energy. Our computed ground state can be explained as the localized Fe(III),Fe(II),Fe(III),Cu(II). As mentioned earlier, a Cu(III) state in these clusters is considered highly unlikely, and we may suggest a re-evaluation of the experimental data.

***[$Cu_2Fe_2S_4$].*** These clusters also have close-lying spin states and changing coupling schemes. The reduced state, computed to be $M_S = 1/2$, is explained as having antiferromagnetically coupled iron sites (one slightly more oxidized than the other), with a total $S = 1/2$, down-coupling with a 2Cu(II) of $S = 1$. The asymmetry between irons indicates that both the $2Fe^{2.5}$ and localized Fe(II),Fe(III) configurations contribute. The oxidized state has all three configurations within 9 kJ/mol of each other; therefore, no conclusion can be drawn on its precise electronic structure, although a mixture of spin states is anticipated. The most stable configuration shown in Tables 1 and 4 has localized low-spin ferric sites, which is unusual.

***[$ZnFe_3S_4$].*** The Zn sites are redox-inactive in all of the studied Zn-containing clusters, with spin densities of zero. This makes these clusters very instructive for calibrating the analysis of other clusters, as assignment of the remaining iron configurations is simpler. It can be anticipated that the [$ZnFe_3S_4$] clusters will resemble [$Fe_3S_4$] clusters in terms of spin coupling, that is, leaving one iron site uncoupled with a final spin corresponding to that site, explaining the observed $S = 5/2$ and 2 for reduced and oxidized states.[52] Our calculations are fully consistent with these observations, from the ground-state energies in Table 1, the separation to higher $M_S$ values, and from spin densities. Thus, the reduced state has a valence-delocalized $2Fe^{2.5}$ site (3.50/3.50) plus a ferrous site with smaller spin density, −2.99, with the additional electron exactly corresponding to a +1 unpaired electron in the $2Fe^{2.5}$ moiety. The oxidized state has two spin-up Fe(III) sites and one spin-down Fe(II) sites, with the $2Fe^{2.5}$ + Fe(III) formulation being consistent with the total spin but with higher $M_S$ values contributing as well (in particular, the all-localized contributions). In the hyperoxidized state, Zn is still closed-shell Zn(II), but one of the three ferric irons is partly intermediate spin. We computed a $M_S = 3/2$ ground state, but configurations are too close in energy to be conclusive.

***[$Zn_2Fe_2S_4$].*** The dizinc clusters, like the other diheterometallic clusters, have never been studied before, although their electronic structures are very clean and can be predicted to be similar to the [$Fe_2S_2$] iron−sulfur clusters in terms of spin, that is, exhibiting full antiferromagnetic coupling. Our computations give reduced and oxidized states with the expected $M_S$ values of 1/2 and 0, respectively, and with comfortable separations of 56 and 45 kJ/mol to the higher $M_S$ configurations. Furthermore, both Zn atoms are clearly redox-inactive, and both irons are clearly antiferromagnetically coupled, as seen from the spin densities. Also, the difference in spin of the two iron sites is consistent with the formal oxidation states, indicating Fe(III)-Fe(II) in the reduced state (−3.21/3.65), equivalent Fe(III) in the oxidized state (−3.52/3.53), and an unusual and interesting valence-localized Fe(III),Fe(IV) system in the hyperoxidized state. In comparison with other structures discussed here, this electronic structure is reasonable, although spin densities up to 0.31 on sulfur atoms indicate that they contribute to being oxidized through a covalent multiconfigurational ground state.

***[$PdFe_3S_4$].*** The unusual Pd-containing clusters, which we describe here, have already been discussed in terms of their trigonally and tetragonally distorted structures. However, despite these unusual geometries, the clusters display spin couplings quite similar to those found in the Ni clusters. The reduced state implies two equivalent iron atoms (3.25/3.25), that is, a mixture

of some Pd(I),2Fe(III),Fe(II) and some Pd(II),2$Fe^{2.5}$,Fe(II), and Pd apparently has some redox activity like the Ni clusters. The oxidized state has four distinct sites with Pd now closer to closed-shell Pd(II) and some mixture of intermediate and high-spin ferrous and ferric iron configurations. Covalency effects appear to be large as judged from the spin delocalization and the distinct sites, even in the formally 3Fe(III) site of the hyperoxidized cluster, again illustrating the difference between first- and second-row transition metals.

***[$Pd_2Fe_2S_4$].*** All of the dipalladium clusters have full antiferromagnetic coupling, as was also the case for the [$Ni_2Fe_2S_4$] clusters, even though geometries are widely different. Furthermore, because of these distortions, all sites are found to be nonequivalent in all oxidation states. However, the general observation that the two remaining iron sites couple antiferromagnetically to each other holds true here as well. Thus, we can conclude that [$Co_2Fe_2S_4$] and, to some extent, [$Cu_2Fe_2S_4$] were the only clusters that did not consistently display this tendency. The reduced state can be described as a mixture of Pd(I),Pd(II),Fe(III),Fe(III) and Pd(II),Pd(II),Fe(III),Fe(II), explaining why spin densities do not differ so much between the sites. This mixture of configurations carries on in the oxidized state, with the electron taken from both configurations. All of these sites are fully localized because of the distorted geometries.

## Concluding Remarks

This article has reported state-of-the-art density functional computations of a number of mainly never-before-characterized iron−sulfur clusters with heterometals Cr, Mn, Co, Ni, Cu, Zn, and Pd, in several redox and spin states. The relationship between electronic structure and how it defines the function (spin states, reduction potentials, reorganization energies) is essential for the rational design of new molecular systems using these cluster types as templates in, for example, proteins.

For clusters that have been characterized experimentally, we obtain mean absolute errors of 0.024 Å for bond lengths ([$Fe_4S_4$], [$NiFe_3S_4$], [$CoFe_3S_4$]) and 0.09 V for reduction potentials relative to the [$Fe_4S_4$] cluster and spin states in general agreement with experiment, except for the interesting case of [$CuFe_3S_4$]. This indicates that the computed properties of the other clusters are of comparable accuracy.

All clusters, except the Pd clusters, form stable cuboidal structures based on tetrahedral coordination environments. Another general and important conclusion is that the structural, redox, and electron-transfer properties described with the given accuracy here span a wide range and are thus providing a good starting point in a search for new molecular systems consisting of clusters with heterometals (substitution reactions), alternative ligands (first-sphere amino acid mutations), and scaffolds (mutations and protein scaffold design). In particular, many modified clusters have closer-lying spin states than the all-iron clusters and are thus expected to have small energy barriers to spin crossover.

A main conclusion of biological relevance is that, in contrast to other electron-transfer sites, that is, cytochromes, blue-copper proteins, and smaller iron−sulfur clusters, the [$Fe_4S_4$] clusters are very insensitive to metal substitution, displaying very small changes in reorganization energies and reduction potentials upon mono- or disubstitution. Thus, the [$Fe_4S_4$] clusters have a clear evolutionary advantage in being robust to pollution from other metals, still retaining function.

**Acknowledgment.** This work was made possible by the Velux Foundation through a Villum−Kann−Rasmussen fellowship, by the Danish Technical Research Council, Grant No. 274-07-0444, and by the Danish Center for Scientific Computing (DCSC) through a computing grant.

**Supporting Information Available:** Tables summarizing the accuracy of the procedure by comparison to larger basis sets and functionals B3LYP and TPSSh (Tables S1−S4) as well as optimized metal−ligand bond lengths for all clusters (Table S5). This material is available free of charge via the Internet at http://pubs.acs.org.

## References and Notes

(1) Beinert, H.; Holm, R. H.; Münck, E. *Science* **1997**, *277*, 653–659.
(2) Johnson, M. K.; Smith, A. D. In *Encyclopedia of Inorganic Chemistry*, 2nd ed.; King, B. B., Ed.; 2005.
(3) Rees, D. C.; Howard, J. B. *Science* **2003**, *300*, 929–931.
(4) Johnson, M. K.; Duderstadt, R. E.; Duin, E. C. *Adv. Inorg. Chem.* **1999**, *47*, 1–82.
(5) Emptage, M. H.; Kent, T. A.; Huynh, B. H.; Rawlings, J.; Orme-Johnson, W. H.; Münck, E. *J. Biol. Chem.* **1980**, *255*, 1793–1796.
(6) Kent, T. A.; Huynh, B. H.; Münck, E. *Proc. Natl. Acad. Sci. U.S.A.* **1980**, *77*, 6574–6576.
(7) Siegbahn, P. E. M. *Adv. Chem. Phys.* **1996**, *93*, 333–387.
(8) Ziegler, T. *Chem. Rev.* **1991**, *91*, 651–667.
(9) Frenking, G.; Frohlich, N. *Chem. Rev.* **2000**, *100*, 717–774.
(10) Jensen, K. P.; Roos, B. O.; Ryde, U. *J. Chem. Phys.* **2007**, *126*, 014103.
(11) Siegbahn, P. E. M.; Blomberg, M. R. A. *Chem. Rev.* **2000**, *100*, 421–437.
(12) Siegbahn, P. E. M. *J. Biol. Inorg. Chem.* **2006**, *11*, 695–701.
(13) Jensen, K. P. *J. Inorg. Biochem.* **2006**, *100*, 1436–1439.
(14) Harrison, J. F. *Chem. Rev.* **2000**, *100*, 679–716.
(15) Neese, F. *J. Biol. Inorg. Chem.* **2006**, *11*, 702–711.
(16) Jensen, K. P.; Ryde, U. *J. Phys. Chem. A* **2003**, *107*, 7539–7545.
(17) Jensen, K. P.; Ryde, U. *Mol. Phys.* **2003**, *13*, 2003–2018.
(18) Jensen, K. P.; Ryde, U. *J. Biol. Chem.* **2004**, *279*, 14561–14569.
(19) Jensen, K. P.; Roos, B. O.; Ryde, U. *J. Inorg. Biochem.* **2005**, *99*, 45–54.
(20) Jensen, K. P. *J. Inorg. Biochem.* **2008**, *102*, 87–100.
(21) Jensen, K. P.; Ooi, B. L.; Christensen, H. E. M. *Inorg. Chem.* **2007**, *46*, 8710–8716.
(22) Torres, R. A.; Lovell, T.; Noodleman, L.; Case, D. A. *J. Am. Chem. Soc.* **2003**, *125*, 1923–1936.
(23) Kennepohl, P.; Solomon, E. I. *Inorg. Chem.* **2003**, *42*, 689–695.
(24) Dey, A.; Glaser, T.; Moura, J. J.-G.; Holm, R. H.; Hedman, B.; Hodgson, K. O.; Solomon, E. I. *J. Am. Chem. Soc.* **2004**, *126*, 16868–16878.
(25) Mouesca, J.-M.; Chen, J. L.; Noodleman, L.; Bashford, D.; Case, D. A. *J. Am. Chem. Soc.* **1994**, *116*, 11898–11914.
(26) Stephens, P. J.; Jollie, D. R.; Warshel, A. *Chem. Rev.* **1996**, *96*, 2491–2513.
(27) Sigfridsson, E.; Olsson, M. H. M.; Ryde, U. *Inorg. Chem.* **2001**, *40*, 2509–2519.
(28) Sigfridsson, E.; Olsson, M. H. M.; Ryde, U. *J. Phys. Chem. B* **2001**, *105*, 5546–5552.
(29) Kennepohl, P.; Solomon, E. I. *Inorg. Chem.* **2003**, *42*, 696–708.
(30) Machonkin, T. E.; Westler, W. M.; Markley, J. L. *Inorg. Chem.* **2005**, *44*, 779–797.
(31) Noodleman, L.; Case, D. A.; Aizman, A. *J. Am. Chem. Soc.* **1988**, *110*, 1001–1005.
(32) Noodleman, L.; Norman, J. G. *J. Chem. Phys.* **1979**, *70*, 4903–4906.
(33) Noodleman, L.; Lovell, T.; Liu, T.; Himo, F.; Torres, R. A. *Curr. Opin. Chem. Biol.* **2002**, *6*, 259–273.
(34) Noodleman, L.; Peng, C. Y.; Case, D. A.; Mouesca, J.-M. *Coord. Chem. Rev.* **1995**, *144*, 199–244.
(35) Becke, A. D. *Phys. Rev. A* **1988**, *38*, 3098–3100.
(36) Perdew, J. P. *Phys. Rev. B* **1986**, *33*, 8822–8824.
(37) Alrichs, R.; Bär, M.; Häser, M.; Horn, H.; Kölmel, C. *Chem. Phys. Lett.* **1989**, *162*, 165–169.
(38) Schäfer, A.; Horn, H.; Ahlrichs, R. *J. Chem. Phys.* **1992**, *97*, 2571–2577.
(39) Cramer, C. J. *Essentials of Computational Chemistry: Theories and Models*; John Wiley & Sons: New York, 2002.
(40) Grafenstein, J.; Cremer, D. *Mol. Phys.* **2001**, *99*, 981–989.
(41) Young, D. *Computational Chemistry: A Practical Guide for Applying Techniques to Real World Problems*; Wiley-VCH: New York, 2001; Chapter 27.

(42) Klamt, A.; Schüürmann, J. *J. Chem. Soc., Perkin Trans.* **1993**, *2*, 799–805.
(43) Schäfer, A.; Klamt, A.; Sattel, D.; Lohrenz, J. C. W.; Eckert, F. *Phys. Chem. Chem. Phys.* **2000**, *2*, 2187–2193.
(44) Honig, B.; Nicholls, A. *Science* **1995**, *268*, 1144–1149.
(45) Klamt, A.; Jonas, V.; Bürger, T.; Lohrenz, J. C. W. *J. Phys. Chem. A* **1998**, *102*, 5074–5085.
(46) Reiss, H.; Heller, A. *J. Phys. Chem.* **1985**, *89*, 4207–4213.
(47) Davidson, E. R.; Clark, A. E. *Int. J. Quantum Chem.* **2005**, *103*, 1–9.
(48) Staples, C. R.; Dhawan, I. K.; Finnegan, M. G.; Dwinell, D. A.; Zhou, Z.-H.; Huang, H.; Verhagen, M. F. J. M.; Adams, M. W. W.; Johnson, M. K. *Inorg. Chem.* **1997**, *36*, 5740–5749.
(49) Finnegan, M. G.; Conover, R. C.; Park, J.-B.; Zhou, Z.-H.; Adams, M. W. W.; Johnson, M. K. *Inorg. Chem.* **1995**, *34*, 5358–5369.
(50) Conover, R. C.; Kowal, A. T.; Fu, W.; Park, J.-B.; Aono, S.; Adams, M. W. W.; Johnson, M. K. *J. Biol. Chem.* **1990**, *265*, 8533–8541.
(51) Conover, R. C.; Park, J. B.; Adams, M. W. W.; Johnson, M. K. *J. Am. Chem. Soc.* **1990**, *112*, 4562–4564.
(52) Butt, J. N.; Armstrong, F. A.; Breton, J.; George, S. J.; Thomson, A. J.; Hatchikian, E. C. *J. Am. Chem. Soc.* **1991**, *113*, 6663–6670.
(53) Hagen, W. R.; Van den Berg, W. A. M.; Van Dongen, W. M. A. M.; Reijerse, E. J.; Van Kan, P. J. M. *J. Chem. Soc., Faraday Trans.* **1998**, *94*, 2969–2973.
(54) Venkateswara, P.; Holm, R. H. *Chem. Rev* **2004**, *104*, 527–559; Compounds 30 and 31.
(55) Zhou, J.; Scott, M. J.; Hu, Z.; Peng, G.; Munck, E.; Holm, R. H. *J. Am. Chem. Soc.* **1992**, *114*, 10843–10854.
(56) Brereton, P. S.; Verhagen, M. F. J. M.; Zhou, Z. H.; Adams, M. W. W. *Biochemistry* **1998**, *37*, 7351–7362.
(57) Zhou, J.; Raebiger, J. W.; Crawford, C. A.; Holm, R. H. *J. Am. Chem. Soc.* **1997**, *119*, 6242–6250.
(58) Marcus, R. A.; Sutin, N. *Biochim. Biophys. Acta* **1985**, *811*, 265–322.

JP8014782